

Iterative Image Reconstruction From Projections Based On Generalised Kaiser-Bessel Window Functions

Filip Jacobs and Ignace Lemahieu

University of Ghent
Sint-Pietersnieuwstraat 41
B-9000 Ghent, Belgium
jacobs@petultra.rug.ac.be

Abstract - Tomographic images are calculated from data provided by a scanner. The reconstruction algorithms used for this purpose are either analytical or iterative in nature. The paper focuses on an iterative algorithm called the row-action maximum-likelihood algorithm, and on transmission tomography. Iterative algorithms approximate the image as a linear combination of a limited set of basis functions. The paper introduces a new set of basis functions, called blobs, into the field of process tomography. It also presents preliminary results of a study which evaluates the advantage of using blobs, instead of pixels, for different amounts of available data and different noise levels. The results clearly show that the use of blobs is also beneficial for process tomography.

Keywords : tomography, reconstruction, projection, blobs

1. INTRODUCTION

Tomographic scanners allow us to investigate inaccessible areas of an industrial process by performing external measurements. Each measurement is related to the spatial distribution of a physical quantity in and around that area. The physical quantity depends on the scanning configuration and may be the local density of a positron-emitting tracer [1], the local linear attenuation coefficient for ultrasonic waves [2] or x-rays [3], etc. By using an appropriate scanning configuration, one is able to reconstruct, from the measurements, an image representing the physical quantity in a two dimensional plane through the industrial process.

The methods used to reconstruct the images are either analytical or iterative in nature. Analytical algorithms [4] are fast, but their disadvantage is that they are not able to precisely model the physics and statistical characteristics of the data acquisition process. In process tomography one often encounters a situation where the data elements are noisy and where only a moderate amount of data is available. In such situations it is better to use iterative algorithms [5] which are slower but can better cope with noisy data and an inadequate sampling of the measurement space.

Iterative algorithms represent the image as a linear combination of a limited set of basis functions $b_j(r)$, with appropriate coefficients v_j , i.e.

$$f(r) = \sum_{j=1}^J v_j b_j(r). \quad (1)$$

The basis functions are often chosen to be pixels (in 2D) or voxels (in 3D). However, recent studies [6,7,8] have shown that more appropriate basis functions exist. In section 2 we introduce generalised Kaiser-Bessel window functions as basis functions into the field of process tomography. These are circular basis functions which are spatially limited and effectively frequency limited.

During the reconstruction process an iterative algorithm calculates the optimal coefficient values $\mathbf{v} = [v_1 \dots v_J]^t$ according to a certain criterion. The criterion depends on the scanner and on the goals one wants to achieve. The paper focuses on transmission tomography, where the expected values $\boldsymbol{\mu} = [\mu_1 \dots \mu_i]^t$ of the measurements \mathbf{d} are related to line-integrals over the image,

$$\mu_i = \int_{L_i} f(r) dr = \sum_{j=1}^J p_{i,j} v_j, \quad (2)$$

with L_i a scanner-dependent line, and

$$p_{i,j} = \int_{L_i} b_j(r) dr. \quad (3)$$

The measurements are, for instance, obtained by measuring the total attenuation suffered by a thin acoustic wave or a thin bundle of x-rays while

propagating through the industrial process, or by detecting photon pairs which are generated along the connecting line of two detectors. Photon pairs appear when a positron emitting tracer is used and electrons are available. These tracers emit positrons which subsequently annihilate with a nearby electron while generating a photon pair.

According to the presence or absence of noise one has to use a different optimisation criterion. Whenever, for instance, x-ray sources are used one can neglect the presence of noise and assume that each measurement d_i is predicted by its expected value. The reconstruction algorithm then tries to solve (2) by minimising a certain functional. For example, in the ART algorithm it is the Cartesian distance between the available data \mathbf{d} and the expected measurements $\boldsymbol{\mu}$ for a given image (determined by eq. (2)) [9],

$$\arg \left[\min_v \sqrt{\sum_{j=1}^J (d_j - \mu_j)^2} \right]. \quad (4)$$

When positron emitters are used one cannot neglect the presence of noise and has to use a stochastic Poisson-model for the measurement process. A Poisson process is completely determined by its expected value. We assume that the measurements are statistically independent. The reconstruction algorithm is then designed in order to maximise the a posteriori probability density function

$$P(f(\mathbf{r})) \prod_{i=1}^I P(d_i | f(\mathbf{r})), \quad (5)$$

with $P(f(\mathbf{r}))$ the prior which determines the probability that a certain image will be measured before any measurements are performed, and

$$P(d_i | f(\mathbf{r})) = \frac{(\mu_i)^{d_i}}{d_i!} \exp(-\mu_i), \quad (6)$$

the Poisson probability that d_i photon pairs are detected given the image. The actual formulation of the prior can be based on the maximum entropy principle [10,11] or Markov random fields [12,13]. Algorithms which assume that each image has the same probability of being measured neglect the prior, resulting in an algorithm which maximises the likelihood of the image. In the paper we focus on such an algorithm, called the row-action maximum-likelihood algorithm (RAMLA).

The paper presents a numerical observer study which compares the performance of the RAMLA algorithm when it is implemented with

pixels on the one hand, and blobs on the other hand. We hereby define a statistical ensemble of software phantoms and several figures of merit (FOMs). An FOM is a numerical value which reflects the ability of a person or a machine to perform a certain task. The task we are interested in is distinguishing areas with high and low intensities versus background activity, with a 15 percent difference. The distinction is made with a pixel-based method and two thresholds. The thresholds and the reconstruction parameters are optimised for different amounts of available data, and different noise levels. The optimal parameter values are subsequently used to evaluate the reconstruction algorithms. For different software phantoms we generate the corresponding FOMs and determine the statistical difference between both methods with the Wilcoxon signed rank test for paired data. The results are summarised in section 5.

2. GENERALISED KAISER BESSEL WINDOW FUNCTIONS

Generalised Kaiser-Bessel window functions were introduced into the field of medical tomography in 1990 by Robert Lewitt [6]. He used them to reconstruct three dimensional (3D) positron emission tomography (PET) [14] images with iterative reconstruction algorithms. He called them blobs. Since then their usage has been optimised thoroughly to reconstruct both 2D [8] and 3D [15,16] PET images. In both cases they have shown to be superior to pixels and voxels.

Blobs $b_{n,m,a,\alpha}(r)$ depend on four parameters: the dimensionality n of the image (e.g. 2 for 2D), the order m of the "modified Bessel function" of the first kind $I_m(\cdot)$ which is used to define the blob, the radius a of the blob, and the so-called taper-parameter α which determines the global shape of the blob. Small values for α result in wide blobs and large values for α result in blobs having narrow peaks and long tails. They are defined as

$$b(r) = \frac{\left(1 - \left(\frac{\|r\|}{a}\right)^2\right)^{\frac{m}{2}} I_m\left(\alpha \sqrt{1 - \left(\frac{\|r\|}{a}\right)^2}\right)}{I_m(\alpha)}$$

for $\|r\| < a$ and 0 elsewhere. Note that this equation does not depend on the dimensionality of the image because the function values only depend on the norm of the argument. The parameter values have to be optimised according to the data characteristics. However, the optimisation procedure requires a lot of computer power [8] and we wanted to perform evaluations corresponding to 9 different data characteristics. Therefore, we decided to use only one blob. Its

profile and power spectral density are shown in Figure 1 and 2, respectively.

3. THE RAMLA ALGORITHM

The row-action maximum-likelihood algorithm is an iterative reconstruction algorithm which maximises the likelihood of the image (see section 1). It was published in 1996 by Browne and De Pierro [17]. The RAMLA algorithm converges faster than the maximum likelihood expectation maximisation [18] and the ordered subset expectation maximisation [19] algorithms. Recent comparative studies have shown that the RAMLA algorithm performs best among these three algorithms for the reconstruction of 3D PET images with [8] and without [7] the use of Fourier rebinning [20].

The RAMLA algorithm processes the data elements sequentially. The order in which they are processed has its influence on the quality of the reconstructed image. By using k to denote the iteration number and i_k to denote the data element to be processed during the k -th iteration, we can formulate one RAMLA iteration as follows

$$v_j^{k+1} = v_j^k + \lambda^k v_j^k \left(\frac{d_{i_k}}{\sum_{n=1}^J p_{i_k,n} v_n^k} - 1 \right) p_{i_k,j} \quad (7)$$

with λ^k a relaxation parameter which determines the weight given to the update. Large values to allow heavy updates and small values to allow only slight modifications of the current estimate. Note that only a few coefficient values have to be altered per iteration, namely the ones that correspond to basis functions which are intersected by the i -th line.

4. TRAINING AND EVALUATION

In order to compare two reconstruction methods we need to define a protocol. We modified the methodology proposed in [21,22] which is designed to train and evaluate reconstruction algorithms for medical 3D PET images. We first define the task we want to perform. We want to evaluate the ability of a person to distinguish areas with high and low intensities versus background activity in a given reconstructed image. Areas showing a high, low and background activity are referred to as hot, cold and normal spots, respectively. The task and the evaluation is not performed by a person but by a numerical observer, i.e. a computer. Therefore, we have to translate the task and the evaluation into mathematical formulas.

The task is numerically performed by using two thresholds, one for cold and one for hot spots. Pixel values lower than the cold spot threshold are considered to belong to a cold spot. Pixel values higher than the hot spot threshold are considered to belong to a hot spot. The residual pixels are considered to belong to the background. The thresholds are optimised during the training procedure.

The ability to perform the task has to be translated into one or more figures of merit (FOMs). The higher its value the better a person is able to perform the task, according to our model. The pixels which correspond to a true hot, normal and cold spots are denoted by H_r , N_r and C_r . They are determined by the software phantoms. The pixels which are assumed to be hot, normal and cold, after applying the above mentioned decision algorithm, are denoted by H_a , N_a and C_a . The number of elements in a set is determined by the $N(\cdot)$ operator. The hot and cold spot sensitivity reflects the ability of a person to detect hot and cold spots,

$$sensh = N(H_a \cap H_r) / N(H_r), \quad (8)$$

$$senc = N(C_a \cap C_r) / N(C_r). \quad (9)$$

The hot and cold spot specificity reflects the ability of a person to select hot and cold spots without selecting pixels corresponding to another type of spot,

$$spech = N(H_a \cap H_r) / N(H_a), \quad (10)$$

$$specc = N(C_a \cap C_r) / N(C_a). \quad (11)$$

These FOMs should be as large as possible. Their maximum value is one and their minimum value is zero. If one wants to be certain that a feature certainly appears, then one should maximise the sensitivity. If one only wants to detect a specific feature, then one should maximise the specificity. The optimal balance between these two extremes is determined by the costs associated with wrong decisions. In this paper we used the compromise that each wrong decision is equally bad.

We designed a statistically defined ensemble of 2D software phantoms. Each software phantom consists of a randomly chosen number of non-overlapping disks which are positioned randomly over the field of view and have randomly chosen radii. The dimensions of the images is 64 by 64 (see Figure 3). The disks are also randomly chosen to represent a hot, a normal or a cold spot. The activity in a hot spot is assumed to be 15 percent higher than its background, a normal spot has the same activity as the background, and a cold spot has an

activity which is assumed to be 15 percent lower than its background. Areas outside the field of view don't contain any activity. The total area covered by the disks lies between 10 and 15 percent of the total area of the field of view. The total amount of activity in the image is scaled to a predefined number, i.e. 10^4 , 10^5 , or 10^6 .

For each software phantom we generated a corresponding data set. Hereby, we calculated the expected values μ_i of the data elements d_i for different lines. The lines were chosen in such a way that we obtained 4, 6 or 8 equally spaced projection angles and 64 samples per projection. Subsequently, we took an element of a Poisson distribution with expected value μ_i and assigned it to the corresponding data element.

With 100 randomly chosen software phantoms, and corresponding data sets, we first determined the optimal thresholds for the decision algorithm. For each disk in these phantoms we calculated the average pixel value. The average values corresponding to hot, normal and cold spots were assumed to be normally distributed. We determined for each kind of activity the average and standard deviation, resulting in three average values and three standard deviations. These values allowed us to determine the optimal thresholds in order to distinguish hot from normal and cold from normal spots. For the cold spot threshold, for instance, we calculated the threshold which resulted in equal probabilities to wrongly assign a certain pixel to a cold and a normal spot, respectively, by using the normal curves obtained for cold and normal spots.

After determining the optimal threshold values we generated 100 new software phantoms and corresponding data sets. With these phantoms we determined the relaxation parameter value of the RAMLA algorithm which resulted in the highest possible FOM value, i.e. we trained the RAMLA algorithm. We assume that three iterations are sufficient to obtain an adequate reconstructed image. This resulted in eight different relaxation parameters, four corresponding to the use of pixels and four corresponding to the use of blobs.

Finally, we generated 25 new phantoms, and corresponding data sets, in order to compare the usage of pixels to blobs. Hereby, we calculated for each software phantom the corresponding eight FOMs. Furthermore, we calculated the average values of these FOMs over the several software phantoms, and determined the statistical significance of the difference between the obtained average FOMs with the Wilcoxon signed rank test for paired data.

We applied the above explained training and evaluation protocol to determine the improvement we obtain by using blobs instead of pixels for the reconstruction of a transmission tomogram with the RAMLA algorithm. We performed this evaluation for 3 different amounts of data, i.e. 4, 6, or 8 projection angles and 64 samples per projection, and different amounts of activity, i.e. 10^4 , 10^5 , or 10^6 counts. The amount of activity also determines the noise level. The higher the activity the lower the noise level.

5. RESULTS

In Table 1 we summarised the average sensitivities and specificities for hot and cold spots. The obtained total ranks are also presented in Table 1. A total rank smaller than 89, 77 and 68 corresponds to a statistical significance of 0.025, 0.01 and 0.005, respectively. The significant differences are highlighted.

Table 1 clearly shows the improvement we obtain by using blobs to determine the hot and cold spot sensitivity, and the hot spot specificity. For the cold spot specificity we do not obtain any improvement. On the contrary we find that in some cases the use of pixels is significantly better than the use of blobs. This might be altered by using more appropriate thresholds.

The images in Figure 3 show the visual improvement we obtain by using blobs for the case of 6 projection angles and 10^5 counts.

6. FIGURES AND TABLES

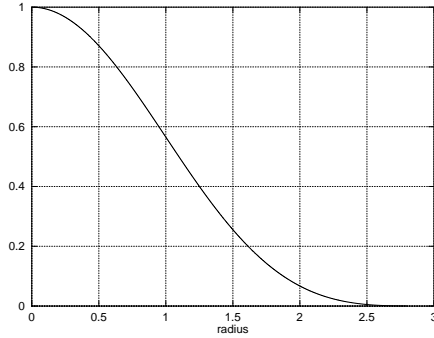


Figure 1 : Profile of a blob

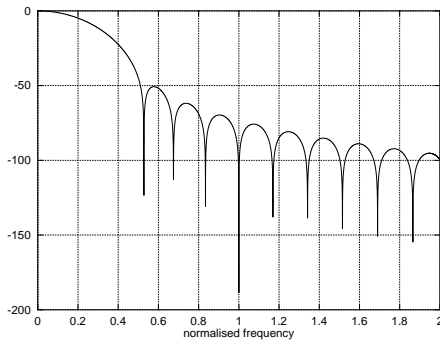


Figure 2 : Spectral density of a blob

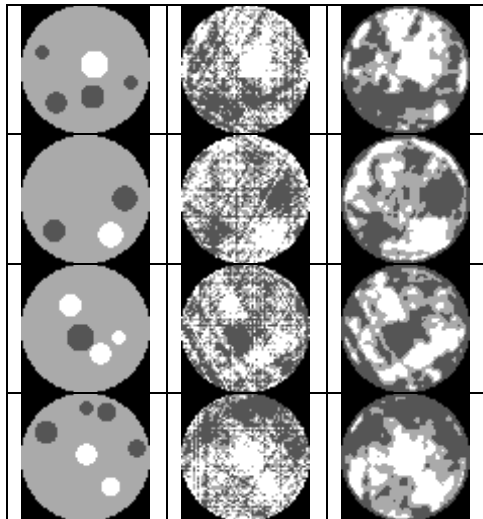


Figure 3 : Examples of software phantoms (left) with the reconstructed images based on pixels (middle) and blobs (right) after classifying each pixel as belonging to a hot, normal or cold spot. Dark spots represent a low activity and light spots a high activity.

sensh	1,E+04	1,E+05	1,E+06
4	0,715	0,902	0,959
	0,570	0,788	0,956
	46	22	140
6	0,692	0,978	0,994
	0,588	0,901	0,991
	67	15	142
8	0,698	0,992	0,998
	0,614	0,927	0,995
	63	9	84

sensc	1,E+04	1,E+05	1,E+06
4	0,745	0,903	0,961
	0,661	0,793	0,940
	113	37	33
6	0,741	0,956	0,992
	0,662	0,887	0,994
	85	32	160
8	0,782	0,984	0,999
	0,686	0,952	0,994
	46	47	44

spech	1,E+04	1,E+05	1,E+06
4	0,155	0,272	0,402
	0,117	0,213	0,232
	81	110	51
6	0,181	0,239	0,219
	0,109	0,230	0,195
	33	142	115
8	0,193	0,230	0,256
	0,126	0,320	0,202
	50	110	52

specc	1,E+04	1,E+05	1,E+06
4	0,121	0,190	0,188
	0,103	0,161	0,253
	99	133	9
6	0,115	0,187	0,171
	0,123	0,204	0,204
	131	148	119
8	0,134	0,180	0,164
	0,124	0,206	0,202
	126	141	43

Table 1 : The average sensitivities and specificities for blobs (top) and pixels (middle) and the ranked sums for paired data (bottom) for different amounts of total activity, i.e. 10^4 , 10^5 and 10^6 , and a different number of equidistant projection angles, i.e. 4, 6 and 8. Highlighted total sums correspond to a statistical significance of 0.025 percent (the threshold equals 89).

REFERENCES

- [1] D. Parker, A. Dijkstra, and P. McNeil, "Positron emission particle tracking studies of granular flow in a rotating drum", in *Process Tomography 1995, Implementation for Industrial Processes*, (Bergen, Norway).
- [2] G. Brown, D. Reilly, and D. Mills, "Ultrasonic transmission-mode tomography applied to gas/solids flow", in *Process Tomography 1995, Implementation for Industrial Processes*, (Bergen, Norway).
- [3] D. Toye, P. Marchot, M. Crine, and G. L'Homme, "Analysis of liquid flow distribution in trickle bed reactor using computer assisted tomography", in *Process Tomography 1995, Implementation for Industrial Processes*, (Bergen, Norway).
- [4] R. M. Lewitt, "Reconstruction algorithms: Transform methods", *Proceedings of the IEEE*, vol. 71, pp. 390-408, March 1983.
- [5] Y. Censor, "Finite series-expansion reconstruction methods", *Proceedings of the IEEE*, vol. 71, pp. 409-419, March 1983.
- [6] R. M. Lewitt, "Multidimensional digital image representations using generalized kaiser-bessel window functions", *J. Opt. Soc. Am.*, vol. 7, pp. 1834-1846, October 1990.
- [7] S. Matej and J. A. Browne, "Performance of a fast maximum likelihood algorithm for fully 3D PET reconstruction" in *Series Computational Imaging and Vision: Three-dimensional Image Reconstruction in Radiology and Nuclear Medicine* (P. Grangeat and J.-L. Amans, eds.), pp. 297-316, Kluwer Academic Publishers, 1996.
- [8] F. Jacobs, S. Matej, and R. Lewitt, "Image reconstruction techniques for PET", August 1998. Department of Electronics and Information Systems, University of Ghent, Medical Image and Signal Processing group, Technical Report R9810 and Department of Radiology, University of Pennsylvania, Medical image processing group technical report No. MIPG245.
- [9] R. Gordon, "A tutorial on ART", *IEEE Transactions on Nuclear Science*, vol. 21, pp. 78-93, June 1974.
- [10] P. Desmedt, Bayesian image reconstruction in positron emission tomography (in Dutch). PhD thesis, University of Ghent, 1995.
- [11] P. Desmedt and I. Lemahieu, "A comparison of different prior laws for bayesian image reconstruction in positron emission tomography", in *Maximum Entropy and Bayesian Methods, Proceedings of MAXENT92*, (France), pp. 393-398, 1992.
- [12] E. Sundermann, Simulated Annealing for the reconstruction of positron emission tomography images (in Dutch). PhD thesis, University of Ghent, march 1998.
- [13] E. Sundermann and I. Lemahieu, "PET image reconstruction using simulated annealing", in *Proceedings: SPIE -- The International Society for Optical Engineering*, vol. 2434, (San Diego, California), pp. 378-386, February 1995. *Medical Imaging 1995 - Image Processing*.
- [14] J. D. Bronzino and co., *The Biomedical Engineering Handbook*. A CRC Handbook Published in Cooperation with IEEE Press, 1995.
- [15] R. M. Lewitt, "Alternatives to voxels for image representation in iterative reconstruction algorithms", *Phys. Med. Biol.*, vol. 37, no. 3, pp. 705-716, 1992.
- [16] S. Matej and R. M. Lewitt, "Practical considerations for 3D image reconstruction using spherically symmetric volume elements", *IEEE Transactions on Medical Imaging*, vol. 15, pp. 68-78, February 1996.
- [17] J. A. Browne and A. R. De Pierro, "A row-action alternative to the EM algorithm for maximizing likelihoods in emission tomography", *IEEE Transactions on Medical Imaging*, vol. 15, no. 5, pp. 687-699, 1996.
- [18] L. A. Shepp and Y. Vardi, "Maximum likelihood reconstruction for emission tomography", *IEEE Transactions on Medical Imaging*, vol. 1, pp. 113-122, October 1982.
- [19] H. M. Hudson and R. S. Larkin, "Accelerated image reconstruction using ordered subsets of projection data", *IEEE Transactions on Medical Imaging*, vol. 13, pp. 601-609, December 1994.
- [20] M. DeFrise, R. Clack, and D. W. Townsend, "Topical review: Image reconstruction from truncated, two-dimensional, parallel projections", *Inverse Problems*, vol. 11, pp. 287-313, 1995.
- [21] S. S. Furuie, G. T. Herman, T. K. Narayan, P. E. Kinahan, J. S. Karp, R. M. Lewitt, and S. Matej, "A methodology for testing for statistically significant differences between fully 3D PET reconstruction algorithms", *Phys. Med. Biol.*, vol. 39, pp. 341-354, 1994.
- [22] S. Matej, S. S. Furuie, and G. T. Herman, "Relevance of statistically significant differences between reconstruction algorithms", *IEEE Transactions on Image Processing*, vol. 5, pp. 554-556, March 1996.